SIAM J. IMAGING SCIENCES
Vol. 4, No. 1, pp. 57–78

Directional Multiscale Amplitude and Phase Decomposition by the Monogenic Curvelet Transform*

Martin Storath†

Abstract. We reconsider the continuous curvelet transform from a signal processing point of view. We show that the analyzing elements of the curvelet transform, the curvelets, can be understood as analytic signals in the sense of the partial Hilbert transform. We then generalize the usual curvelets by the monogenic curvelets, which are analytic signals in the sense of the Riesz transform. They yield a new transform, called the monogenic curvelet transform. This transform has the useful property that it behaves at the fine scales like the usual curvelet transform and at the coarse scales like the monogenic wavelet transform. In particular, the new transform is highly anisotropic at the fine scales and yields a well-interpretable amplitude/phase decomposition of the transform coefficients over all scales. We illustrate the advantage of this new directional multiscale amplitude/phase decomposition for the estimation of directional regularity.

Key words. curvelet transform, analytic signal, monogenic signal, Hilbert transform, Riesz transform, directional wavelet transform

AMS subject classifications. 42C40

DOI. 10.1137/100803924

1. Introduction.

Analytic wavelets are important in one-dimensional signal processing, because they yield a meaningful multiscale decomposition of a signal into amplitude and phase, where the amplitude has the interpretation of the envelope of the signal. This fact is exploited for AM-demodulation, for instance [8]. In one dimension, analytic wavelets are easily constructed by just taking a real wavelet ψ and adding the *Hilbert transform* of ψ as an imaginary part.

However, the construction of two-dimensional analytic wavelets is not straightforward, and several approaches have been made. Kingsbury constructed analytic wavelets by a separable approach, called the *dual tree complex wavelet transform* [13]. These analytic wavelets proved to be a powerful tool in many image processing applications such as denoising or image rotation [13, 18]. However, the dual tree complex wavelet transform still has, as a separable construction, an intrinsically one-dimensional character. Nonseparable wavelet constructions are in general more flexible and better adapted to the two-dimensional structure of images. In order to construct nonseparable analytic wavelets one has to generalize the Hilbert transform to two dimensions. A straightforward construction is the *partial Hilbert transform*. Unfortunately, the partial Hilbert transform is again some kind of separable construction; thus it has several drawbacks, which we will point out in section 2.2.1.

*Received by the editors July 29, 2010; accepted for publication (in revised form) November 5, 2010; published electronically January 20, 2011.
http://www.siam.org/journals/siims/4-1/80392.html
†M6 - Mathematische Modellbildung, Zentrum Mathematik, Technische Universität München, Boltzmannstr. 3, D-85748 Garching bei München, Germany (storath@ma.tum.de).

A more suitable nonseparable construction of analytic wavelets in two dimensions uses the *Riesz transform*. These Riesz transform based analytic wavelets are called *monogenic wavelets*. Several authors already use such monogenic wavelets in image processing [9, 16, 21], for example, in applications such as AM/FM analysis [21] or descreening [9]. The mother wavelets used in [9] and [21] are completely isotropic [9] or near-isotropic [21], and directionality is imposed only by the Riesz transforms. However, the analysis of orientations is often an important task in image processing, e.g., for edge detection and analysis. To gain higher anisotropy, Unser and Van De Ville propose in [22] *higher order Riesz transforms*, which lead to an approach similar to the steerable pyramid. Olhede and Metikas gain anisotropy by a certain directional wavelet transform [16]. However, the degree of anisotropy of all three approaches does not adapt to the scale, so the resolution of the orientations of the singularities still has some uncertainty [4]. Using the words of [4], these wavelet transforms do not resolve the so-called *wavefront set*, which is the set of singularities of a function along with their (possibly multiple) orientations.

The *continuous curvelet transform (CCT)*, proposed by Candès and Donoho in [4], resolves the orientations of the singularities exactly, hence *without* any uncertainty. To use again the words of [4], the curvelet transform does resolve the *wavefront set*. This is possible because the curvelet transform increases the anisotropy of its analyzing elements—the *curvelets*—as the scale decreases according to a *parabolic scaling law*. Thus, the curvelets have higher directional selectivity at the fine scales. In order to construct a directional monogenic wavelet transform, it seems natural to take the curvelet transform as a basis. We mention that the curvelet transform is not the only such transform; a similar construction was proposed in [10], for example. Interestingly, by construction the curvelets are already analytic wavelets in the sense of the partial Hilbert transform. To overcome the problems that arise from the partial Hilbert transform, we propose in this article *monogenic curvelets* and define the *monogenic curvelet transform (MCT)*. The new MCT unifies the advantages of the monogenic wavelet transform and the excellent directional selectivity of the usual curvelet transform.

The article is organized as follows. First, we give an introduction to the analytic signal and its generalizations to two dimensions, namely, the analytic signal in the sense of the Hilbert transform and the monogenic signal. We show how they yield reasonable amplitude/phase decompositions (section 2). We then identify the usual curvelets as analytic wavelets in the sense of the Hilbert transform (section 3). In section 4 we construct new monogenic curvelets and define the MCT. This is achieved by replacing the usual curvelets by the new monogenic curvelets. We prove that the CCT and the MCT converge uniformly to each other at the fine scales, and we illustrate the differences at the coarse scales (section 5). After a view on the frame discretization in section 6, we present a possible application, namely, estimation of regularity from the amplitude of the MCT coefficients.

1.1. Preliminaries and notation. Throughout this article we use (r, ω) for polar coordinates in the frequency domain, and $x = (x_1, x_2)$ and $\xi = (\xi_1, \xi_2)$ for Cartesian coordinates in the spatial domain and in the frequency domain, respectively. The space of real-valued square-integrable functions is denoted by $L^2(\mathbb{R}^n, \mathbb{R})$. Unless otherwise stated, all formulas hold in the L^2-sense, thus almost everywhere (a.e.). f is always a real-valued and square-integrable function; thus $f \in L^2(\mathbb{R}^n, \mathbb{R})$, where $n = 1, 2$. ρ_θ denotes a counterclockwise rotation in $\mathbb{R}^2$ by the angle θ with its matrix realization

$$\rho_\theta = \begin{pmatrix} \cos\theta & -\sin\theta \\ \sin\theta & \cos\theta \end{pmatrix}.$$

The translation by $b \in \mathbb{R}^2$ is denoted by τ_b. We denote the corresponding rotation and translation operators with the same symbols, that is,

$$\rho_\theta f(x) := f(\rho_\theta^{-1} x) = f(\rho_{-\theta} x),$$
$$\tau_b f(x) := f(x - b).$$

The complex imaginary unit is denoted by the (italic) letter i. We denote the modulation by $e_\xi(x) := e^{2\pi i\, \xi \cdot x}$ and define the Fourier transform by

$$\widehat{f}(\xi) = \mathcal{F} f(\xi) = \int_{\mathbb{R}^n} f(x) e^{-2\pi i\, \xi \cdot x}\, dx.$$

2. Analytic signal concepts. We give a brief introduction to the analytic signal in one dimension and its generalizations to two dimensions. We will call every generalization of the analytic signal to two dimensions an *analytic signal* as well. A short overview of amplitude/phase decomposition by analytic signals is given at the end of the section.

2.1. The analytic signal in one dimension. Let $\mathcal{H} : L^2(\mathbb{R}, \mathbb{R}) \to L^2(\mathbb{R}, \mathbb{R})$ be the *Hilbert transform* defined in the Fourier domain by

$$\widehat{\mathcal{H} f}(s) = i\, \operatorname{sign}(s)\, \widehat{f}(s). \tag{2.1}$$

Note that $\mathcal{H} f$ is real-valued. Recall that we are in the L^2-setting, so (2.1) has to be understood a.e. Thus it does not matter how the sign-function is defined in 0.

A complex-valued function $g : \mathbb{R} \to \mathbb{C}$ whose imaginary part is the Hilbert transform of its real part, that is, $\operatorname{Im} g = -\mathcal{H}(\operatorname{Re} g)$, is called an *analytic signal*. The function $f - i\,\mathcal{H} f$ is an example of an analytic signal. In one-dimensional signal processing the analytic signal is used to decompose a signal into *amplitude* and *phase*, or, loosely spoken, into a signal intensity and a signal structure. We refer the reader to [8, 11, 12] for exhaustive discussions of the Hilbert transform and its applications to one-dimensional signal processing.

2.2. The analytic signal in two dimensions. We now present two reasonable extensions of the one-dimensional analytic signal to two dimensions, the *Hilbert-analytic signal* and the *monogenic signal*. We will give evidence that the latter is preferable. As the underlying concept of these extensions is the analytic signal, we also refer to both the Hilbert-analytic signal and the monogenic signal by the more abstract name *analytic signal*.

2.2.1. The Hilbert-analytic signal. A straightforward extension to two dimensions is achieved by letting the Hilbert transform operate on parallel lines which point towards a fixed orientation θ. This extension is called *partial Hilbert transform with respect to the angle* θ [2], defined in the Fourier domain for $f \in L^2(\mathbb{R}^2, \mathbb{R})$ by

$$\widehat{\mathcal{H}_\theta f}(\xi) = i\, \operatorname{sign}(\cos(\theta)\xi_1 + \sin(\theta)\xi_2)\, \widehat{f}(\xi).$$

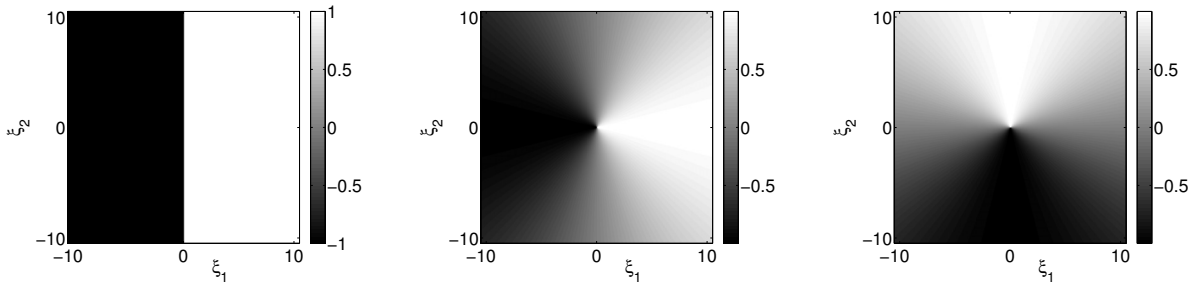

(a) $\operatorname{sign} \xi_1$ (b) $\frac{\xi_1}{|\xi|}$ (c) $\frac{\xi_2}{|\xi|}$

Figure 1. *Fourier multipliers (imaginary parts) of partial Hilbert transform* $\mathcal{H}_0$ (a) *and Riesz transforms* $\mathcal{R}_1$ (b) *and* $\mathcal{R}_2$ (c). *The origin of the coordinate system lies in the center of the images.*

The Fourier multiplier of the Hilbert transform $\mathcal{H}_0$ is displayed in Figure 1(a). We call a complex-valued function $g : \mathbb{R}^2 \to \mathbb{C}$ an *analytic signal in the sense of the partial Hilbert transform* (or *Hilbert-analytic signal*) if its imaginary part is the partial Hilbert transform with respect to any angle θ of its real part, that is, $\operatorname{Im} g = -\mathcal{H}_\theta(\operatorname{Re} g)$.

The Hilbert-analytic signal has two major drawbacks. The first is that the partial Hilbert transform has a purely one-dimensional nature; thus, the Hilbert-analytic signal does not sufficiently take into account the structure of true two-dimensional signals. The second problem is the dependence on the angle θ. One encounters the problem of choosing a suitable angle $\theta \in [0, 2\pi)$. Though there are functions f which allow only one sensible choice for θ, in general, $\mathcal{H}_\theta$ yields a different analytic signal of f for every different angle θ.

Let us illustrate another problem of the partial Hilbert transform concerning the decay rate. Let $f \in L^2(\mathbb{R}^2, \mathbb{R})$ such that $\widehat{f} \in C^\infty$ and such that $\widehat{f}$ is supported in a ring around the origin; that is, $\operatorname{supp} \widehat{f} = \overline{B_R(0)} \setminus B_r(0)$ with $R > r > 0$. As $\widehat{f} \in C^\infty$, we get that f is of rapid decay; that is, $f \in o(|x|^{-m})$ for every $m \in \mathbb{N}$. The application of the partial Hilbert transform to f generates a step singularity in $\widehat{f}$, so $\widehat{\mathcal{H}_\theta f}$ loses its differentiability, independently of the choice of θ. Hence, $\mathcal{H}_\theta f$ is not of rapid decay any longer.

Later we will need the following properties of the partial Hilbert transform.

Lemma 2.1.

(1) *The (unrotated) partial Hilbert transform* $\mathcal{H}_0$ *commutes with the translation operator* τ_b*; that is,*

$$\tau_b \mathcal{H}_0 f = \mathcal{H}_0 \tau_b f.$$

(2) $\mathcal{H}_\theta$ *can be interchanged with the rotation* ρ_θ *by the following intertwining relation:*

$$\rho_\theta \mathcal{H}_0 f = \mathcal{H}_\theta \rho_\theta f.$$

Proof.

(1) Using the modulations $e_{-b}(\xi) = e^{-2\pi i\, \xi \cdot b}$, the statement follows from

$$\mathcal{F}\left(\tau_b \mathcal{H}_0 f\right)(\xi) = \widehat{\mathcal{H}_0 f}(\xi) e_{-b}(\xi) = i \operatorname{sign}(\xi) \widehat{f}(\xi) e_{-b}(\xi) = i \operatorname{sign}(\xi) \widehat{\tau_b f}(\xi) = \mathcal{F}\left(\mathcal{H}_0 \tau_b f\right)(\xi).$$

(2) We use the fact that the rotation commutes with the Fourier transform

$$\begin{aligned}\mathcal{F}\left(\rho_\theta \mathcal{H}_0 f\right)(\xi) &= \rho_\theta \widehat{\mathcal{H}_0 f}(\xi) = \widehat{\mathcal{H}_0 f}(\rho_\theta^{-1}\xi) \\ &= \widehat{\mathcal{H}_0 f}\left(\begin{pmatrix} \cos(\theta)\xi_1 + \sin(\theta)\xi_2 \\ -\sin(\theta)\xi_1 + \cos(\theta)\xi_2 \end{pmatrix}\right) \\ &= i\ \mathrm{sign}(\cos(\theta)\xi_1 + \sin(\theta)\xi_2)\rho_\theta \widehat{f}(\xi) \\ &= \mathcal{F}\left(\mathcal{H}_\theta \rho_\theta f\right)(\xi). \qquad \blacksquare\end{aligned}$$

2.2.2. The monogenic signal. In order to overcome the aforementioned drawbacks, another generalization of the analytic signal for two dimensions, which is called the *monogenic signal*, was introduced in [7]. It is considered to be the proper generalization of the one-dimensional-analytic signal for image processing [7] and has proved its usefulness in several image processing applications [9, 21, 22]. The monogenic signal is based on the *Riesz transform*. For $f \in L^2\left(\mathbb{R}^2, \mathbb{R}\right)$ the Riesz transform with respect to the axis x_ν, $\nu = 1, 2$, is defined in the L^2-sense by

$$\widehat{\mathcal{R}_\nu f}(\xi) = i\,\frac{\xi_\nu}{|\xi|}\widehat{f}(\xi). \tag{2.2}$$

Like f, $\mathcal{R}_\nu f$ is a real-valued L^2-function, that is, $\mathcal{R}_\nu : L^2\left(\mathbb{R}^2, \mathbb{R}\right) \to L^2\left(\mathbb{R}^2, \mathbb{R}\right)$; see [19]. The Fourier multipliers of the Riesz transforms are displayed in Figure 1(b)–(c). Unlike the partial Hilbert transform, the Riesz transform does not depend on any orientation θ. Instead we have *two* transforms $\mathcal{R}_1 f$ and $\mathcal{R}_2 f$ with respect to the fixed coordinate axes x_1 and x_2. Consequently, a proper representation of the monogenic signal needs *two* imaginary parts, one for $\mathcal{R}_1 f$ and one for $\mathcal{R}_2 f$. Hence we have to switch from the complex numbers to a hypercomplex algebra which possesses at least two algebraically independent imaginary units. The classical choice for such a hypercomplex algebra are the quaternions

$$\mathbb{H} := \left\{h = a + \mathbf{i}\,b + \mathbf{j}\,c + \mathbf{k}\,d : a, b, c, d \in \mathbb{R}\right\},$$

which are an extension of the complex numbers with the three imaginary units $\mathbf{i}$, $\mathbf{j}$, and $\mathbf{k}$. A short description of the quaternions is given in Appendix A. Now we are able to define the monogenic signal $\mathcal{M}f$ by

$$\mathcal{M}f := f - \mathbf{i}\,\mathcal{R}_1 f - \mathbf{j}\,\mathcal{R}_2 f.$$

The monogenic operator $\mathcal{M}$ maps a real-valued function f to a quaternion-valued function $\mathcal{M}f$; hence $\mathcal{M} : L^2(\mathbb{R}^2, \mathbb{R}) \to L^2(\mathbb{R}^2, \mathbb{H})$.

We will later use the following important properties of the Riesz transform, which were proved in [19].

Lemma 2.2. *Let $f \in L^2(\mathbb{R}^2)$, $\nu = 1, 2$, and let τ_b be the translation operator and ρ_θ the rotation operator. Then the Riesz transforms satisfy the relations*

$$\begin{aligned}\tau_b \mathcal{R}_\nu f &= \mathcal{R}_\nu \tau_b f, \\ \mathcal{R}_1 \rho_\theta f &= \cos(\theta)\rho_\theta \mathcal{R}_1 f + \sin(\theta)\rho_\theta \mathcal{R}_2 f, \\ \mathcal{R}_2 \rho_\theta f &= -\sin(\theta)\rho_\theta \mathcal{R}_1 f + \cos(\theta)\rho_\theta \mathcal{R}_2 f.\end{aligned}$$

2.3. Amplitude/phase decomposition by analytic signals. We briefly introduce the notion of amplitude and phase of the complex numbers and the quaternions in an exemplary way. Deeper treatments of the subject can be found in [8, 9, 12]. To prevent differentiation of cases we define an arcus tangens with two arguments by

$$\operatorname{atan2}(b, a) := \arg(a + i\, b).$$

A complex number $z = u + i\, v$ can be decomposed into an *amplitude* $A_{\mathbb{C}} \in \mathbb{R}_0^+$, a *phase angle* $p_{\mathbb{C}} \in [0, \pi]$, and a *phase orientation* $q_{\mathbb{C}} \in \{-i, i\}$, that is,

$$z = A_{\mathbb{C}} \cdot e^{q_{\mathbb{C}} \cdot p_{\mathbb{C}}}, \tag{2.3}$$

where $A_{\mathbb{C}} = |z|$, $p_{\mathbb{C}} = \operatorname{atan2}(|\operatorname{Im} z|, \operatorname{Re} z)$, and $q_{\mathbb{C}} = i \operatorname{sign}(\operatorname{Im} z) = i \frac{\operatorname{Im} z}{|\operatorname{Im} z|}$. The real part u is recovered by

$$u = \operatorname{Re} z = \operatorname{Re}(A_{\mathbb{C}} \cdot e^{q_{\mathbb{C}} \cdot p_{\mathbb{C}}}) = A_{\mathbb{C}} \cos(p_{\mathbb{C}}).$$

Analogously to the complex decomposition, we define, for a quaternion h, amplitude by $A_{\mathbb{H}} = |h|$ and phase angle by $p_{\mathbb{H}} = \operatorname{atan2}(|\operatorname{Im} h|, \operatorname{Re} h)$. Note that the quaternionic phase orientation $q_{\mathbb{H}} = \frac{\operatorname{Im} h}{|\operatorname{Im} h|}$ is purely imaginary. Thus, a quaternion is decomposed as

$$h = A_{\mathbb{H}} \cdot e^{q_{\mathbb{H}} \cdot p_{\mathbb{H}}}, \tag{2.4}$$

and the real part is recovered by

$$a = \operatorname{Re} h = \operatorname{Re}(A_{\mathbb{H}} \cdot e^{q_{\mathbb{H}} \cdot p_{\mathbb{H}}}) = A_{\mathbb{H}} \cos(p_{\mathbb{H}}).$$

We omit the subscripts $\mathbb{C}$ or $\mathbb{H}$ in the following.

The most important advantage of analytic signals is that they provide a reasonable notion of amplitude and phase of real-valued function $f(x)$. Let us clarify first in which cases we consider an amplitude/phase decomposition as reasonable. The amplitude function $A(x)$ should represent the signal intensity. $A(x)$ should vary slowly, such that $A(x)$ becomes insensitive with respect to small shifts. The phase function $p(x)$ should encode the oscillatory part of $f(x)$, which is the part that is sensitive to small shifts of the signal.

We first consider a naive amplitude/phase decomposition of a real-valued (thus nonanalytic) signal $f : \mathbb{R} \to \mathbb{R}$, so

$$f(x) = |f(x)| \operatorname{sign} f(x) = |f(x)|\, e^{i \arg f(x)} = A(x) e^{q(x) \cdot p(x)}.$$

The amplitude boils down to the absolute value $A(x) = |f(x)|$, the phase angle $p(x) = \arg f(x) \in \{0, \pi\}$ becomes a jump-function between 0 and π, and the phase direction $q_{\mathbb{R}}(x) = i$ remains constant. This approach obviously does not fulfill the expectations of an amplitude/phase decomposition; for instance, the amplitude still contains oscillations (Figure 2(b)–(d)).

We now illustrate that the analytic signal, on the other hand, yields a reasonable amplitude/phase decomposition. As the analytic signal $f(x) - i\, \mathcal{H} f(x)$ is a true complex-valued function, we get according to (2.3) the decomposition

$$f(x) - i\, \mathcal{H} f(x) = A(x) e^{q(x) \cdot p(x)}.$$

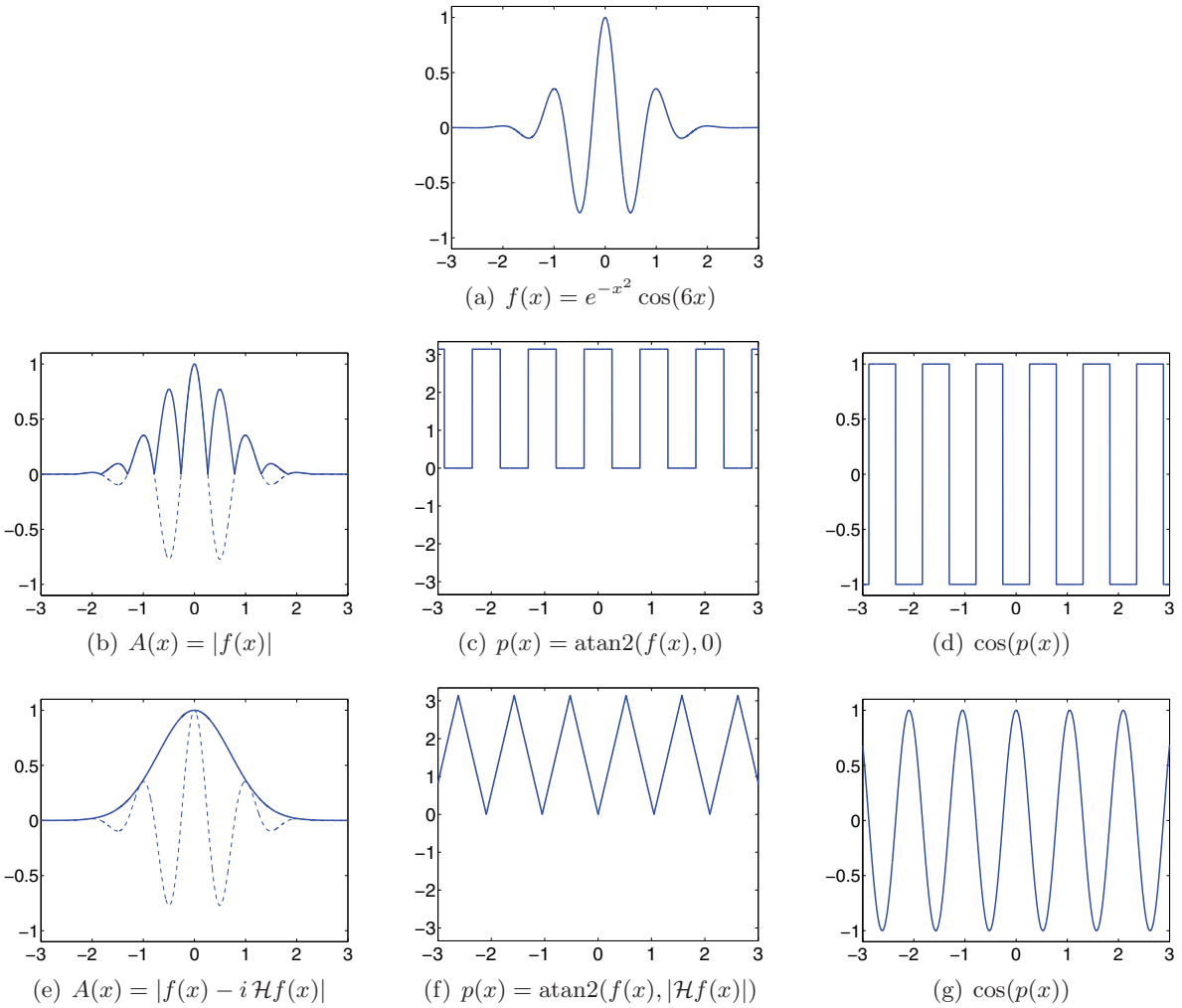

Figure 2. *Oscillatory signal* (a) *and the real (second row) and analytic (third row) amplitude/phase decompositions. The real amplitude/phase decomposition mixes up the envelope and the oscillating part* (b)*. In contrast, the analytic amplitude/phase decomposition clearly separates the oscillation from the slowly varying envelope* (e)–(g)*. The thin dashed lines in* (b) *and* (e) *show the original function* f*.*

The amplitude now has the interpretation of a slowly varying envelope, and the cosine of the phase encodes the oscillation part of the signal (Figure 2(e)–(g)).

Analogous arguments hold for the analytic signal of a two-dimensional function $f : \mathbb{R}^2 \to \mathbb{R}$. For the complex-valued Hilbert-analytic signal $f(x) - i\,\mathcal{H}_\theta f(x)$, we can take the same amplitude/phase decomposition of the one-dimensional case. For the quaternion-valued monogenic signal $\mathcal{M}f(x) = f(x) - \mathbf{i}\,\mathcal{R}_1 f(x) - \mathbf{j}\,\mathcal{R}_2 f(x)$, we have the slight difference that we need the quaternionic amplitude/phase decomposition according to (2.4). Examples of the monogenic amplitude/phase decomposition will be given in section 5.

3. The curvelet transform as analytic signal.

We first recall the definition of the continuous curvelet transform (CCT) as proposed in [4]. We then prove that the curvelets are by

construction analytic signals in the sense of the partial Hilbert transform.

3.1. The usual continuous curvelet transform (CCT). Let $W : \mathbb{R}_0^+ \to \mathbb{R}_0^+$ be a compactly supported radial window function and $V : \mathbb{R} \to \mathbb{R}_0^+$ be a compactly supported angular window function satisfying the *admissibility conditions*

$$\int_0^\infty W(ar)^2 \frac{1}{a}\, da = 1 \quad \forall r > 0 \tag{3.1}$$

and

$$\int_{-1}^{1} V(u)^2\, du = 1. \tag{3.2}$$

Examples of admissible windows W and V are given in [14]. Let $a \in \mathbb{R}^+$, $b \in \mathbb{R}^2$, and $\theta \in [0, 2\pi)$. Recall that (r, ω) denote polar coordinates in the frequency domain. A *curvelet* $\gamma_{ab\theta}$ is defined by

$$\gamma_{ab\theta}(x) = \gamma_{a00}(\rho_\theta(x - b)) = \rho_{-\theta}\tau_b\gamma_{a00}(x),$$

where ρ_θ is a rotation as defined in section 1.1 and γ_{a00} is defined by its Fourier transform

$$\widehat{\gamma}_{a00}(r, \omega) = a^{3/4} W(ar) V\left(\frac{\omega}{\sqrt{a}}\right). \tag{3.3}$$

The angular windowing is well defined only for scales a smaller than a fixed scale α_0 [4]. Thus for the coarser scales $a \geq \alpha_0$ the transform is continued by a purely radial window

$$\widehat{\gamma}_{a00}(r, \omega) = a \frac{W(ar)}{\sqrt{\pi}}. \tag{3.4}$$

The *CCT* Γ_f of a function f is defined by

$$\Gamma_f : \begin{cases} \mathbb{R}^+ \times \mathbb{R}^2 \times [0, 2\pi) & \to \mathbb{C}, \\ (a, b, \theta) & \mapsto \langle \gamma_{ab\theta}, f \rangle . \end{cases} \tag{3.5}$$

Note that $\gamma_{ab\theta}$ is complex-valued for $a < \alpha_0$ and real-valued for $a \geq \alpha_0$.

3.2. Interpretation of curvelets as Hilbert-analytic signals. We show that $\gamma_{ab\theta}$ is by construction a Hilbert-analytic signal for $a < \alpha_0$. To this end, we define the real-valued function β_{a00} by symmetrizing $\widehat{\gamma}_{a00}$ with respect to the origin in the Fourier domain

$$\widehat{\beta}_{a00}(\xi_1, \xi_2) := \frac{1}{2}(\widehat{\gamma}_{a00}(\xi_1, \xi_2) + \widehat{\gamma}_{a00}(-\xi_1, -\xi_2)).$$

Now the simple calculation (omitting the subscripts)

$$\widehat{\gamma}(\xi_1, \xi_2) = \widehat{\beta}(\xi_1, \xi_2) - i\,(i\ \mathrm{sign}(\xi_1)\widehat{\beta}(\xi_1, \xi_2)) = \widehat{\beta}(\xi_1, \xi_2) - i\,\widehat{\mathcal{H}_0\beta}(\xi_1, \xi_2)$$

yields $\gamma_{a00} = \beta_{a00} - i\,\mathcal{H}_0\beta_{a00}$. By the translation invariance and the rotation covariance of the partial Hilbert transform (Lemma 2.1), we get that $\gamma_{ab\theta}$ is a Hilbert-analytic signal; that is,

$$\gamma_{ab\theta} = \mathrm{Re}\,\gamma_{ab\theta} + i\ \mathrm{Im}\,\gamma_{ab\theta} = \beta_{ab\theta} - i\,\mathcal{H}_{-\theta}\beta_{ab\theta}. \tag{3.6}$$

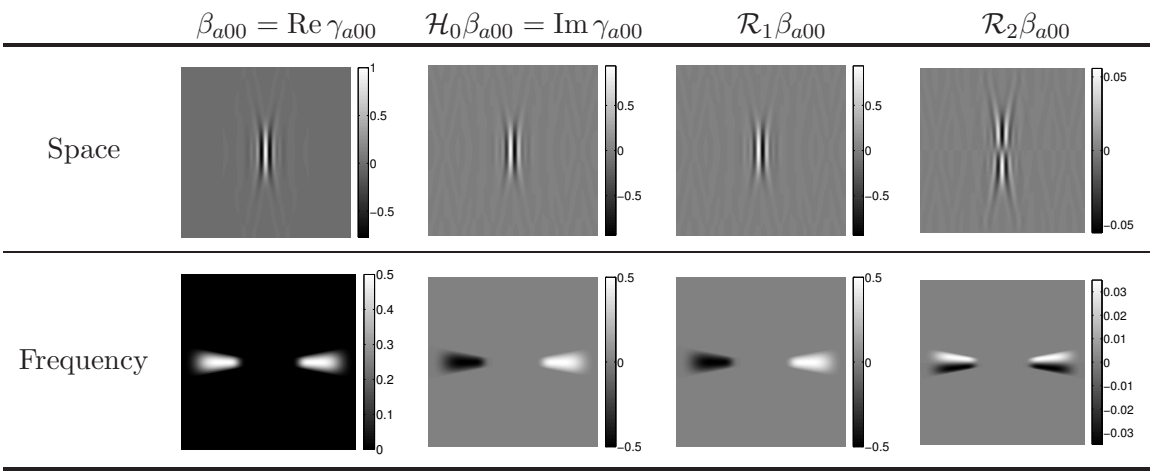

Figure 3. *Comparison of the atoms of the CCT and the MCT at a fine scale. There is no visible difference between* $\mathcal{H}_0\beta_{a00}$ *and* $\mathcal{R}_1\beta_{a00}$*. Note that the values of* $\mathcal{R}_2\beta_{a00}(x)$ *are one order of magnitude smaller than those of* $\mathcal{R}_1\beta_{a00}$*.*

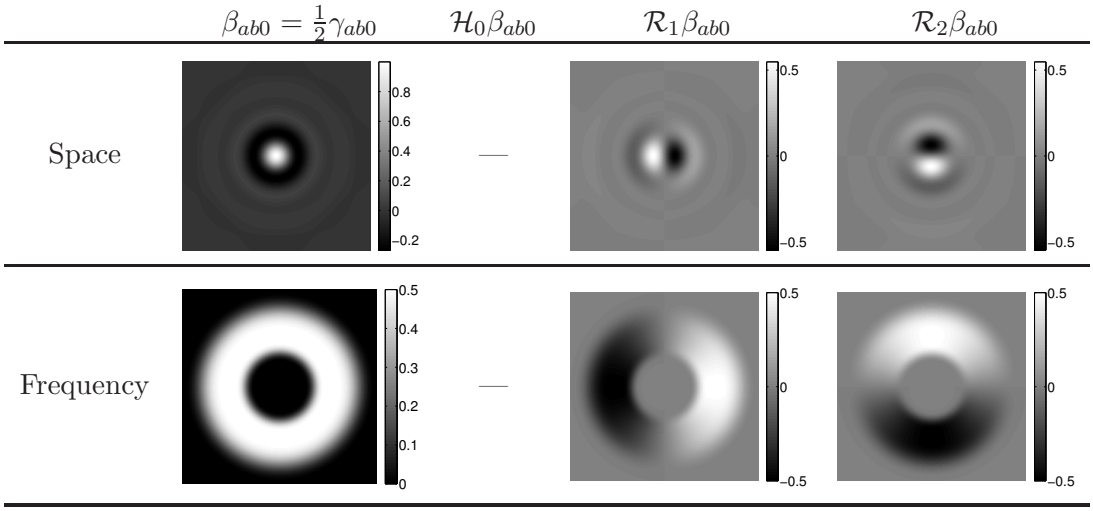

Figure 4. *Comparison of the atoms of the CCT and the MCT at a coarse scale. The partial Hilbert transform is not sensible for these isotropic functions, so the usual curvelets are not analytic wavelets at the coarse scales. The Riesz transform, on the other hand, is applicable to isotropic functions as well, so the monogenic curvelets are analytic wavelets at the coarse scales.*

Candès and Donoho considered real-valued curvelets in [6] but without establishing this connection to the complex-valued curvelets.

From now on we refer to the usual curvelet transform also as the *Hilbert-analytic curvelet transform*. We call $\beta_{ab\theta}$ *real(-valued) curvelets*. Examples of the usual curvelets for a fine scale can be found in Figure 3 and for a coarse scale in Figure 4.

4. The monogenic curvelet transform (MCT). In the last two sections we introduced the necessary tools to define the new MCT. In section 2.2.2 we stated that the proper gen-

eralization of the one-dimensional analytic signal is not the Hilbert-analytic signal but the monogenic signal. This motivates us to replace the usual curvelets $\gamma_{ab\theta}$, which we identified as Hilbert-analytic wavelets, by *monogenic curvelets* $\mathcal{M}\beta_{ab\theta}$. We construct monogenic curvelets by applying the monogenic signal to the real-valued curvelets $\beta_{ab\theta}$ as defined in section 3, thus adding the Riesz transforms as imaginary parts:

$$\mathcal{M}\beta_{ab\theta} := \mathcal{M}(\beta_{ab\theta}) = \beta_{ab\theta} - \mathbf{i}\,\mathcal{R}_1(\beta_{ab\theta}) - \mathbf{j}\,\mathcal{R}_2(\beta_{ab\theta}).$$

Illustrations of some monogenic curvelets can be found in Figure 3 for a fine scale monogenic curvelet and in Figure 4 for a coarse scale monogenic curvelet. The monogenic curvelets yield a new quaternion-valued transform, which we call *monogenic curvelet transform (MCT)*. We define the *MCT* M_f by

$$M_f : \begin{cases} \mathbb{R}^+ \times \mathbb{R}^2 \times [0, 2\pi) & \to \mathbb{H}, \\ (a, b, \theta) & \mapsto \langle \mathcal{M}\beta_{ab\theta}, f \rangle\,, \end{cases} \tag{4.1}$$

where

$$\langle \mathcal{M}\beta_{ab\theta}, f\rangle = \langle \beta_{ab\theta}, f\rangle + \mathbf{i}\,\langle \mathcal{R}_1(\beta_{ab\theta}), f\rangle + \mathbf{j}\,\langle \mathcal{R}_2(\beta_{ab\theta}), f\rangle\,.$$

Remark 4.1. *For the definition of* M_f *we do not require that* $f \in L^2(\mathbb{R}^2)$. *We require only that* f *be a tempered distribution, because* $\beta_{ab\theta}$ *and* $\mathcal{R}_\nu\beta_{ab\theta} \in \mathcal{S}(\mathbb{R}^2)$.

Like the CCT [5], the MCT has a reproducing formula and a Parseval formula.

Theorem 4.1. *Let* $f \in L^2(\mathbb{R}^2, \mathbb{R})$. *The monogenic curvelets have a Calderón-like reproducing formula*

$$\mathcal{M}f(x) = \int \langle \mathcal{M}\beta_{ab\theta}, f\rangle\, \mathcal{M}\beta_{ab\theta}(x)\, db\, d\theta\, da/a^3 \tag{4.2}$$

a.e. and a Parseval formula

$$\|f\|_2^2 = \int |M_f(a, b, \theta)|^2\, db\, d\theta\, da/a^3. \tag{4.3}$$

The proof of Theorem 4.1 is similar to the proof in [5] and is given in Appendix B.

5. Comparison of the MCT and the CCT. The goal of this section is to point out the differences and similarities between the CCT and the MCT. To this end, we first compare the function plots of the usual curvelets and the monogenic curvelets. At the fine scales, one immediately recognizes the similarities between the imaginary part of γ_{a00} and $\mathcal{R}_1\beta_{a00}$ (Figure 3). At the coarse scales, on the other hand, there is a big difference, because γ_{a00} lacks an imaginary part for $a \geq \alpha_0$ (Figure 4). In Figure 5, the amplitudes and phases of the CCT and the MCT are compared.

5.1. Uniform convergence of MCT and CCT at fine scales. The MCT is quaternion-valued, whereas the CCT is complex-valued; hence they cannot be compared per se. To

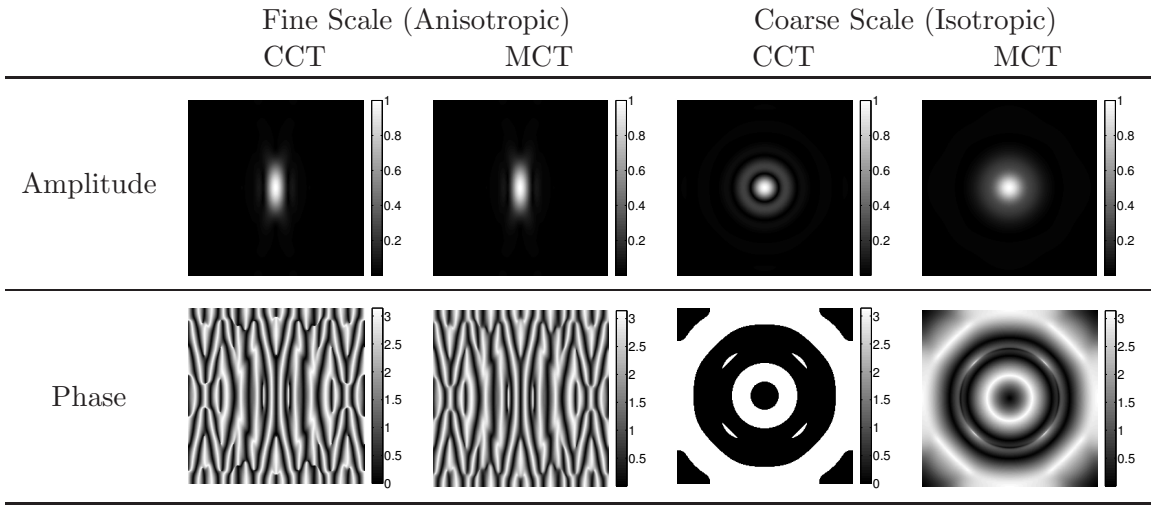

Figure 5. *Comparison of amplitude and phase responses of the filters in Figures 3 and 4. There is no visible difference at the fine scale between CCT and MCT. At the coarse scale the CCT-amplitude oscillates and the CCT-phase is discontinuous, whereas the MCT-amplitude decays monotonously and the MCT-phase is smoother.*

make them comparable, we isometrically embed the complex values of the curvelets into the quaternions. We define the embedded curvelets $\widetilde{\gamma}_{ab\theta}$ by

$$\begin{aligned}\widetilde{\gamma}_{ab\theta} &:= \operatorname{Re}\gamma_{ab\theta} + \mathbf{i}\cos(-\theta)\operatorname{Im}\gamma_{ab\theta} + \mathbf{j}\sin(-\theta)\operatorname{Im}\gamma_{ab\theta}\\ &= \beta_{ab\theta} + \mathbf{i}\cos(-\theta)\mathcal{H}_{-\theta}\beta_{ab\theta} + \mathbf{j}\sin(-\theta)\mathcal{H}_{-\theta}\beta_{ab\theta}\\ &= \beta_{ab\theta} + \mathbf{i}\cos(\theta)\mathcal{H}_{-\theta}\beta_{ab\theta} - \mathbf{j}\sin(\theta)\mathcal{H}_{-\theta}\beta_{ab\theta}.\end{aligned} \tag{5.1}$$

The corresponding embedding of the curvelet coefficients is denoted by

$$\widetilde{\Gamma}_f(a,b,\theta) = \langle \widetilde{\gamma}_{ab\theta}, f\rangle\,.$$

The canonical embedding $\mathbb{C}\to\mathbb{H}$, $a+ib\mapsto a+\mathbf{i}b$ is not suitable here, because it is not compatible with the rotations in this setting. With the embedding (5.1) we are able to prove the uniform convergence of the CCT and the MCT (Corollary 5.4). To this end, we need some preliminary lemmas.

Lemma 5.1. *Let $\Omega_a = ([-\frac{2}{a},-\frac{1}{2a}]\cup[\frac{1}{2a},\frac{2}{a}])\times[-\sqrt{a},\sqrt{a}]$ and β_{a00} be a real curvelet at scale a, where $0<a<\alpha_0$. Then the following statements hold:*

(1) *The support of $\widehat{\beta}_{a00}$ lies in the rectangle Ω_a; that is, $\operatorname{supp}\widehat{\beta}_{a00}\subset\Omega_a$.*

(2) *The measure of $\operatorname{supp}\widehat{\beta}_{a00}$ has the upper bound $\mu(\operatorname{supp}(\widehat{\beta}_{a00}))\le\mu(\Omega_a)=6a^{-1/2}$, where μ denotes the Lebesgue measure.*

(3) $\|\widehat{\beta_{a00}}\|_\infty = a^{3/4}\cdot C_{W,V}$ *with a constant $C_{W,V}$ depending only on the choice of the window functions W and V.*

(4) *For all $\xi\in\Omega_a$ we have the inequalities*

$$\frac{|\xi_2|}{|\xi|}\le 2a^{3/2}$$

and

$$\left|\operatorname{sign}(\xi_1) - \frac{\xi_1}{|\xi|}\right| \leq 2a^{3/2},$$

which are related to the Fourier multiplier of the Riesz transform.

Proof.
(1) The statement holds by construction of $\widehat{\beta}_{a00}$.
(2) $\mu(\Omega_a) = 2(\frac{2}{a} - \frac{1}{2a})(2\sqrt{a}) = 4(\frac{4}{2a} - \frac{1}{2a})\sqrt{a} = 4\frac{3}{2a}\sqrt{a} = 6a^{-1}a^{1/2} = 6a^{-1/2}$.
(3)

$$\left\|\widehat{\beta_{a00}}\right\|_\infty = \sup_{(r,\omega)\in\mathbb{R}^+\times[-1,1]} a^{3/4} W(r)V(\omega) = a^{3/4} \underbrace{\sup_{r\in\mathbb{R}^+} W(r) \sup_{\omega\in[-1,1]} V(\omega)}_{=:C_{W,V}}.$$

(4) The first inequality follows from $|\xi_2| \leq \sqrt{a}$ and $|\xi| \geq \frac{1}{2a}$. For the second we have $|\xi| - |\xi_1| \leq |\xi_1| + |\xi_2| - |\xi_1| = |\xi_2| = \sqrt{a}$; thus it follows that

$$\left|\operatorname{sign}\xi_1 - \frac{\xi_1}{|\xi|}\right| = \left|\frac{\operatorname{sign}\xi_1 |\xi| - \xi_1}{|\xi|}\right| = \left|\frac{|\xi| - |\xi_1|}{|\xi|}\right| \leq \frac{\sqrt{a}}{\frac{1}{2a}} = 2a^{3/2}. \qquad \blacksquare$$

Lemma 5.2. *Let $0 < a < \alpha_0$, $b \in \mathbb{R}^2$, and $\theta \in [0, 2\pi)$. For the L^2-distance of the embedded curvelets $\widetilde{\gamma}_{ab\theta}$ and the monogenic curvelets $\mathcal{M}\beta_{ab\theta}$, there holds the equation*

$$\|\widetilde{\gamma}_{ab\theta} - \mathcal{M}\beta_{ab\theta}\|_2^2 = \|\mathcal{H}_0\beta_{a00} - \mathcal{R}_1\beta_{a00}\|_2^2 + \|\mathcal{R}_2\beta_{a00}\|_2^2.$$

Proof. First we calculate

$$\begin{aligned}
\|\widetilde{\gamma}_{ab\theta} - \mathcal{M}\beta_{ab\theta}\|_2^2 &= \|\beta_{ab\theta} + \mathbf{i}\cos(\theta)\mathcal{H}_{-\theta}\beta_{ab\theta} - \mathbf{j}\sin(\theta)\mathcal{H}_{-\theta}\beta_{ab\theta} - \beta_{ab\theta} - \mathbf{i}\mathcal{R}_1\beta_{ab\theta} + \mathbf{j}\mathcal{R}_2\beta_{ab\theta}\|_2^2 \\
&= \|\mathbf{i}(\cos(\theta)\mathcal{H}_{-\theta}\beta_{ab\theta} - \mathcal{R}_1\beta_{ab\theta}) + \mathbf{j}(-\sin(\theta)\mathcal{H}_{-\theta}\beta_{ab\theta} - \mathcal{R}_2\beta_{ab\theta})\|_2^2 \\
&= \|\cos(\theta)\mathcal{H}_{-\theta}\beta_{ab\theta} - \mathcal{R}_1\beta_{ab\theta}\|_2^2 + \|\sin(\theta)\mathcal{H}_{-\theta}\beta_{ab\theta} + \mathcal{R}_2\beta_{ab\theta}\|_2^2.
\end{aligned}$$

We compute for the first term using Lemmas 2.1 and 2.2

$$\begin{aligned}
\|\cos(\theta)\mathcal{H}_{-\theta}\beta_{ab\theta} - \mathcal{R}_1\beta_{ab\theta}\|_2^2 &= \|\cos(\theta)\mathcal{H}_{-\theta}\rho_{-\theta}\beta_{ab0} - \mathcal{R}_1\rho_{-\theta}\beta_{ab0}\|_2^2 \\
&= \|\cos(\theta)\rho_{-\theta}\mathcal{H}_0\beta_{ab0} - \cos(-\theta)\rho_{-\theta}\mathcal{R}_1\beta_{ab0} + \sin(-\theta)\rho_{-\theta}\mathcal{R}_2\beta_{ab0}\|_2^2 \\
&= \|\rho_{-\theta}[\cos(\theta)(\mathcal{H}_0\beta_{ab0} - \mathcal{R}_1\beta_{ab0}) - \sin(\theta)\mathcal{R}_2\beta_{ab0}]\|_2^2 \\
&= \|\cos(\theta)(\mathcal{H}_0\beta_{ab0} - \mathcal{R}_1\beta_{ab0}) - \sin(\theta)\mathcal{R}_2\beta_{ab0}\|_2^2,
\end{aligned}$$

and analogously for the second term

$$\begin{aligned}
\|\sin(\theta)\mathcal{H}_{-\theta}\beta_{ab\theta} + \mathcal{R}_2\beta_{ab\theta}\|_2^2 &= \|\sin(\theta)\mathcal{H}_{-\theta}\rho_{-\theta}\beta_{ab0} + \mathcal{R}_2\rho_{-\theta}\beta_{ab0}\|_2^2 \\
&= \|\sin(\theta)\rho_{-\theta}\mathcal{H}_0\beta_{ab0} + \sin(-\theta)\rho_{-\theta}\mathcal{R}_1\beta_{ab0} + \cos(-\theta)\rho_{-\theta}\mathcal{R}_2\beta_{ab0}\|_2^2 \\
&= \|\rho_{-\theta}[\sin(\theta)(\mathcal{H}_0\beta_{ab0} - \mathcal{R}_1\beta_{ab0}) + \cos(\theta)\mathcal{R}_2\beta_{ab0}]\|_2^2 \\
&= \|\sin(\theta)(\mathcal{H}_0\beta_{ab0} - \mathcal{R}_1\beta_{ab0}) + \cos(\theta)\mathcal{R}_2\beta_{ab0}\|_2^2.
\end{aligned}$$

Putting both terms together, we get

$$\begin{aligned}
&\|\cos(\theta)(\mathcal{H}_0\beta_{ab0} - \mathcal{R}_1\beta_{ab0}) - \sin(\theta)\mathcal{R}_2\beta_{ab0}\|_2^2 + \|\sin(\theta)(\mathcal{H}_0\beta_{ab0} - \mathcal{R}_1\beta_{ab0}) + \cos(\theta)\mathcal{R}_2\beta_{ab0}\|_2^2 \\
&= \int_{\mathbb{R}^2} (\cos(\theta)(\mathcal{H}_0\beta_{ab0}(x) - \mathcal{R}_1\beta_{ab0}(x)) - \sin(\theta)\mathcal{R}_2\beta_{ab0}(x))^2 + \\
&\quad (\sin(\theta)(\mathcal{H}_0\beta_{ab0}(x) - \mathcal{R}_1\beta_{ab0}(x)) + \cos(\theta)\mathcal{R}_2\beta_{ab0}(x))^2 \, dx \\
&= \int_{\mathbb{R}^2} (\mathcal{H}_0\beta_{ab0}(x) - \mathcal{R}_1\beta_{ab0}(x))^2 + \mathcal{R}_2\beta_{ab0}(x)^2 \, dx \\
&= \|\mathcal{H}_0\beta_{ab0} - \mathcal{R}_1\beta_{ab0}\|_2^2 + \|\mathcal{R}_2\beta_{ab0}\|_2^2 ,
\end{aligned}$$

where the penultimate equation follows from the trigonometric identity

$$(\cos(\theta)u - \sin(\theta)v)^2 + (\sin(\theta)u + \cos(\theta)v)^2 = u^2 + v^2.$$

Now the claim follows because both the Hilbert transform and the Riesz transform commute by Lemmas 2.1 and 2.2 with the translations; that is,

$$\|\mathcal{H}_0\beta_{ab0} - \mathcal{R}_1\beta_{ab0}\|_2^2 + \|\mathcal{R}_2\beta_{ab0}\|_2^2 = \|\mathcal{H}_0\beta_{a00} - \mathcal{R}_1\beta_{a00}\|_2^2 + \|\mathcal{R}_2\beta_{a00}\|_2^2 . \qquad \blacksquare$$

Theorem 5.3. *For every $b \in \mathbb{R}^2$, every $\theta \in [0, 2\pi)$, and every $0 < a < \alpha_0$ it holds that*

$$\|\widetilde{\gamma}_{ab\theta} - \mathcal{M}\beta_{ab\theta}\|_2 \le a^2 4\sqrt{3} C_{W,V},$$

with a constant $C_{W,V}$ depending only on the choice of the window functions W and V.

Proof. From Lemma 5.2, we get

$$\|\widetilde{\gamma}_{ab\theta}(x) - \mathcal{M}\beta_{ab\theta}(x)\|_2^2 = \|\mathcal{H}_0\beta_{a00} - \mathcal{R}_1\beta_{a00}\|_2^2 + \|\mathcal{R}_2\beta_{a00}\|_2^2 . \tag{5.2}$$

Now we estimate upper bounds for the terms in (5.2), so applying the Plancherel equation and using Lemma 5.1 we get

$$\begin{aligned}
\|\mathcal{H}_0\beta_{a00} - \mathcal{R}_1\beta_{a00}\|_2^2 &= \|\mathcal{F}(\mathcal{R}_1\beta_{a00} - \mathcal{H}_0\beta_{a00})\|_2^2 \\
&= \left\| \widehat{\mathcal{R}_1\beta}_{a00} - \widehat{\mathcal{H}_0\beta}_{a00} \right\|_2^2 \\
&= \int_{\mathbb{R}^2} \left| i \, \frac{\xi_1}{|\xi|} \widehat{\beta}_{a00}(\xi) - i \, \operatorname{sign} \xi_1 \widehat{\beta}_{a00}(\xi) \right|^2 d\xi \\
&= \int_{\mathbb{R}^2} \left(\frac{\xi_1}{|\xi|} - \operatorname{sign} \xi_1 \right)^2 \widehat{\beta}_{a00}(\xi)^2 \, d\xi \\
&\le (2a^{3/2})^2 \mu(\operatorname{supp}(\widehat{\beta}_{a00})) \left\| \widehat{\beta}_{a00} \right\|_\infty^2 \\
&= 4a^3 \mu(\operatorname{supp}(\widehat{\beta}_{a00})) \left\| \widehat{\beta}_{a00} \right\|_\infty^2
\end{aligned}$$

and

$$\begin{aligned}\|\mathcal{R}_2\beta_{a00}\|_2^2 &= \left\|\widehat{\mathcal{R}_1\beta_{a00}}\right\|_2^2 \\ &= \int_{\mathbb{R}^2}\left(\frac{\xi_2}{|\xi|}\right)^2 \widehat{\beta}_{a00}(\xi)^2\,d\xi \\ &\le (2a^{3/2})^2\mu(\operatorname{supp}(\widehat{\beta}_{a00}))\left\|\widehat{\beta}_{a00}\right\|_\infty^2 \\ &= 4a^3\mu(\operatorname{supp}(\widehat{\beta}_{a00}))\left\|\widehat{\beta}_{a00}\right\|_\infty^2.\end{aligned}$$

Summing up both terms and applying Lemma 5.1 again, we get

$$\begin{aligned}\|\widetilde{\gamma}_{ab\theta} - \mathcal{M}\beta_{ab\theta}\|_2 &= \sqrt{\|\mathcal{H}_0\beta_{a00} - \mathcal{R}_1\beta_{a00}\|_2^2 + \|\mathcal{R}_2\beta_{a00}\|_2^2} \\ &\le \sqrt{8a^3\mu(\operatorname{supp}(\widehat{\beta}_{a00}))}\left\|\widehat{\beta}_{a00}\right\|_\infty \\ &\le \sqrt{8a^3 6a^{-1/2}}\; a^{3/4}C_{W,V} \\ &= \sqrt{48}a^{8/4}\; C_{W,V} \\ &= a^2 4\sqrt{3}\; C_{W,V},\end{aligned}$$

and the proof is complete. ∎

Corollary 5.4. *Let $f \in L^2(\mathbb{R}^2,\mathbb{R})$. The Hilbert-analytic curvelet coefficients and the monogenic curvelet coefficients converge to each other uniformly in b and θ for $a \to 0$; more precisely,*

$$\left|\widetilde{\Gamma}_f(a,b,\theta) - M_f(a,b,\theta)\right| \le a^2 4\sqrt{3}C_{W,V}\,\|f\|_2\,.$$

Proof. By virtue of the Cauchy–Schwarz inequality we get

$$\begin{aligned}\left|\widetilde{\Gamma}_f(a,b,\theta) - M_f(a,b,\theta)\right| &= |\langle\widetilde{\gamma}_{ab\theta}, f\rangle - \langle\mathcal{M}\beta_{ab\theta}, f\rangle| \\ &= |\langle\widetilde{\gamma}_{ab\theta} - \mathcal{M}\beta_{ab\theta}, f\rangle| \\ &\le \|\widetilde{\gamma}_{ab\theta} - \mathcal{M}\beta_{ab\theta}\|_2\,\|f\|_2 \\ &\le a^2 4\sqrt{3}C_{W,V}\,\|f\|_2\,.\end{aligned}$$ ∎

Corollary 5.4 shows that the CCT and the MCT are essentially the same as the scale a when the scale a is near 0. Thus the asymptotic estimates for $a \to 0$ of the CCT in [4] hold true for the MCT.

5.2. Coarse scale behavior of the MCT. We have seen that CCT and MCT are essentially the same at the fine scales. At the coarse scales, in contrast, the transforms differ strongly. The concept of the Hilbert-analytic signal is not applicable to the isotropic scales (see section 2.2.1). Thus, $\gamma_{ab\theta}$ remains a purely real-valued function for $a \ge \alpha_0$. Hence the amplitude $|\gamma_{ab\theta}|$ boils down to the absolute value of the real numbers. In analogy to the one-dimensional example in Figure 2, the real absolute value $|\gamma_{ab\theta}|$ oscillates and is nonsmooth, even though $\gamma_{ab\theta}$ is smooth (Figure 5, upper row).

Table 1

Comparison between the monogenic wavelets, the usual curvelets, and the monogenic curvelets. Only the monogenic curvelets possess both the high scale-adaptive directionality and a consistent concept of analytic signal over all scales.

	Anisotropy		Analytic signal concept	
	Coarse scales	Fine scales	Coarse scales	Fine scales
Isotropic monogenic wavelets [9, 16]	low	low	monogenic	monogenic
Curvelets [4]	low	high (scale-adaptive)	—	Hilbert-analytic
Monogenic curvelets	low	high (scale-adaptive)	monogenic	monogenic

The concept of the monogenic signal, on the other hand, can be applied to all scales, so $\mathcal{M}\beta_{ab\theta}$ is an analytic signal also at the coarse scales $a \geq \alpha_0$. Following the arguments of section 2.3, $|\mathcal{M}\beta_{ab\theta}|$ can be interpreted as an envelope of $\beta_{ab\theta}$. We observe that $|\mathcal{M}\beta_{ab\theta}|$ is slowly varying and does not oscillate (Figure 5, upper row), whereas the oscillating part is coded in the phase (Figure 5, bottom row)

We want to offer a remark about the connection of the MCT with other existing transforms. Consider the case $\alpha_0 = \infty$. In that case, the angular windowing never applies, so the real parts of the monogenic curvelets are purely isotropic functions. In that case the MCT boils down to the isotropic monogenic wavelet transform of [16] or, after discretization, to the monogenic wavelet frames of [9]. Table 1 depicts the connections we describe in this section.

6. Discretization and frames. We briefly recall the frame discretization of the CCT; details can be found in [5]. The discretization of the MCT derives directly from there. Recall that a family of functions $\{h_i\}_{i\in\mathbb{Z}}$ is called a *tight frame* for $L^2(\mathbb{R}^n)$ if there is an $A > 0$ such that for every $h \in L^2(\mathbb{R}^n)$ there holds

$$A\,\|h\|_2^2 = \sum_{i\in\mathbb{Z}} |\langle h_i, h\rangle|^2\,. \tag{6.1}$$

The usual curvelet family $\gamma_{ab\theta}$ is discretized as follows. The continuous parameters a, b, and θ are replaced by discrete samples, so we set

$$\begin{aligned}
a_j &:= 2^{-j}, \quad j \in \mathbb{Z},\\
\widetilde{a}_j^{1/2} &:= \frac{1}{2}\cdot 2^{-\lfloor j/2\rfloor},\\
\theta_{j,l} &:= \frac{\pi}{2} l \cdot 2^{-\lfloor j/2\rfloor}, \quad \text{where } l = 0,\dots,L_j - 1 \text{ with } L_j := 4\cdot 2^{\lfloor j/2\rfloor},\\
b_{k_1,k_2}^{j,l} &:= \begin{cases} \rho_{\theta_{j,l}}(k_1/2^j, k_2/2^{j/2}) & \text{if } j \geq 0,\\ (k_1/2^j, k_2/2^j) & \text{else,}\end{cases}
\end{aligned}$$

where $(k_1, k_2) \in \mathbb{Z}^2$. The discrete parameters sample the continuous parameters exactly only at every other scale due to the construction of $\widetilde{a}_j$ [5]. The discrete curvelet frame is the family

$$\left\{\varphi_{j,k,l} := \varphi_{j,0,0}(\rho_{\theta_{j,l}}(\cdot - b_{k_1,k_2}^{j,l})) \mid l = 0,\dots,L_j - 1\right\}_{j,k_1,k_2\in\mathbb{Z}},$$

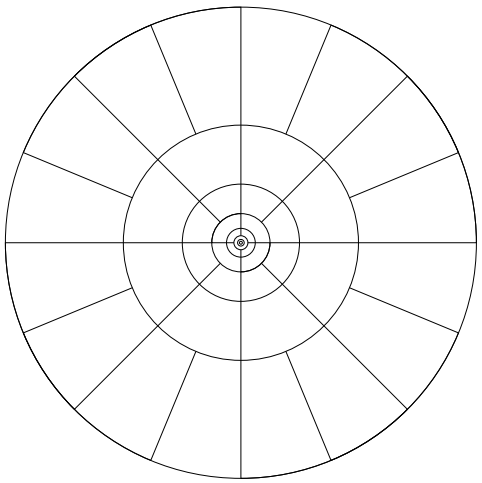

Figure 6. *Schematic tiling of the frequency plane by the curvelet frame.*

where

$$\widehat{\varphi}_{j,0,0}(r,\omega) = \begin{cases} W(a_j r)V\left(\frac{\omega}{\pi \widetilde{a}_j^{1/2}}\right) & \text{if } j \geq 0, \\ W(a_j r) & \text{else.} \end{cases}$$

The curvelet frame yields a tiling of the frequency plane according to the scheme in Figure 6.

Note that now W and V have to fulfill admissibility conditions that are slightly different from those in the continuous case, namely,

$$\sum_{j=-\infty}^{\infty} W(2^j r)^2 = 1 \quad \forall\, r \in (3/4, 3/2)\,,$$
$$\sum_{l=-\infty}^{\infty} V(t-l)^2 = 1 \quad \forall\, t \in (-1/2, 1/2)\,.$$

We derive a frame of monogenic curvelets $\mathcal{M}\psi_{j,k,l}$ in exactly the same fashion as we derived the MCT from the usual curvelet transform in sections 3 and 4. We symmetrize the basic element $\widehat{\varphi}_{j,0,0}$ with respect to the origin by

$$\widehat{\psi}_{j,0,0}(\xi_1,\xi_2) := \frac{1}{2}(\widehat{\varphi}_{j,0,0}(\xi_1,\xi_2) + \widehat{\varphi}_{j,0,0}(-\xi_1,-\xi_2))$$

to get a tight frame of real-valued functions $\psi_{j,k,l}$ [3]. Because of the symmetry it is sufficient to discretize the angles in the range from $[0,\pi)$, so we modify L_j to $\widetilde{L}_j := 2 \cdot 2^{\lfloor j/2 \rfloor}$.

In [9, Theorem 5.1], Held et al. proved that the Riesz transforms maps a frame of real-valued elements into a frame of quaternion-valued elements with the same frame bounds. So it follows that

$$\left\{ \mathcal{M}\psi_{j,k,l} = \psi_{j,k,l} + \mathbf{i}\,\mathcal{R}_2\psi_{j,k,l} + \mathbf{j}\,\mathcal{R}_2\psi_{j,k,l} \mid l = 0,\dots,\widetilde{L}_j - 1 \right\}_{j,k_1,k_2 \in \mathbb{Z}}$$

is also a tight frame for $L^2(\mathbb{R}^2,\mathbb{R})$.

7. Application: Estimation of regularity by decay rates of curvelet coefficients. Let us switch for the moment from the special case of the CCT to continuous wavelet transforms $\mathcal{W}_f$ in general. We assume that the wavelet transforms depend on the parameters a, b, and θ as the curvelet transform does. The decay rate $d_{\theta,b}$ of the wavelet coefficients $\mathcal{W}_f(a,b,\theta)$ for $a \to 0$ can be seen as a measure for the (Hölder-)regularity of a function f. (See [4, 15, 17, 23].) So the regularity at a point b with respect to the orientation θ, denoted by $d_{\theta,b}$, can be estimated from the relation

$$|\mathcal{W}_f(a,b,\theta)| \sim C_{\theta,b} \cdot a^{d_{\theta,b}}. \tag{7.1}$$

To exploit this characterization of regularity in practice, we have to estimate $d_{\theta,b}$ from a limited number of scales a_j, $j = 0, \dots, N$. This can be done by *wavelet coefficient regression*, which is a least squares approach after taking logarithms in (7.1) [1, Chapter 11].

To get a stable estimation of $d_{\theta,b}$, the amplitude $|\mathcal{W}_f(a_j,b,\theta)|$ must behave well for all available scales a_j. We pointed out in section 5 that the amplitude of the CCT oscillates at the isotropic scales (Figure 5). This behavior leads to artifacts in the estimation of the decay rates $d_{\theta,b}$. The MCT in contrast does not suffer from these artifacts (Figure 7).

From a theoretical point of view, only the limit $a_j \to 0$ matters for the estimation of regularity. Thus we compute $d_{\theta,b}$ from the finest scales a_j, which are anisotropic for a sufficiently small a_j. However, there are cases where it makes sense to employ the isotropic scales as well for the estimation. For example, if for some reason (e.g., runtime), the number of directions at the finest scale is small, let us assume only four directions. Then we have only three anisotropic scales available (one scale with four directions and two scales with two directions). Hence the anisotropic scales provide only three data points for the computation of $d_{\theta,b}$, which is not sufficient for a robust estimation of $d_{\theta,b}$. The addition of further data points by using the subsequent isotropic scales leads to a more robust estimation; see Figure 8.

8. Conclusion and outlook. We introduced the MCT, which is a new tool for directional multiscale amplitude/phase decomposition. We took the usual curvelet transform with its excellent directional selectivity and imposed the monogenic signal to add a sensible notion of amplitude and phase to the curvelet coefficients for all scales. The uniform convergence of the MCT to the CCT assures us that the MCT inherits the most important properties of the CCT. A frame discretization was derived directly from the discretization of the usual curvelet transform. We illustrated the advantages of the MCT over the CCT by the estimation of directional regularity.

An extension to three-dimensional functions is more or less straightforward. We construct a three-dimensional CCT analogously to the two-dimensional curvelet transform and impose the Riesz transform in the same way as in the two-dimensional case. A discretized version of a three-dimensional curvelet transform is presented in [24], for example. In the three-dimensional case, we get a third imaginary part $\mathcal{R}_3 f$. As the third imaginary unit of the quaternions $\mathbf{k}$ is not algebraically independent of the others, that is, $\mathbf{k} = \mathbf{i}\,\mathbf{j}$, we have to switch to a hypercomplex algebra with three algebraically independent imaginary units.

Appendix A. The quaternions. The quaternions can be defined as a four-dimensional $\mathbb{R}$-vector space, whose basis, denoted by $\{\mathbf{1}, \mathbf{i}, \mathbf{j}, \mathbf{k}\}$, is a noncommutative algebra with the properties $\mathbf{i}^2 = \mathbf{j}^2 = \mathbf{k}^2 = -1$ and $\mathbf{k} = \mathbf{i}\,\mathbf{j} = -\mathbf{j}\,\mathbf{i}$. As for the complex numbers, a conjugation

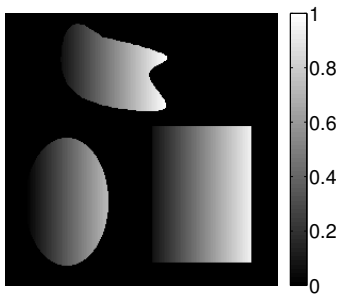

Orientation	Decay rate $d_{\theta,b}$ computed by CCT	Decay rate $d_{\theta,b}$ computed by MCT
$\theta = \frac{\pi}{8}$	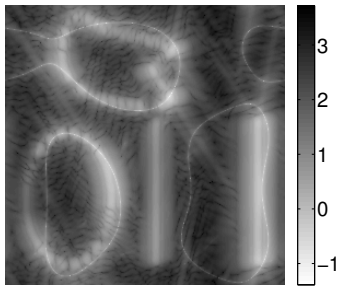	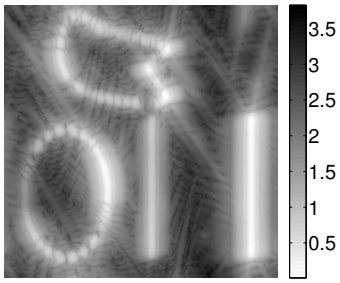
$\theta = \frac{5\pi}{8}$	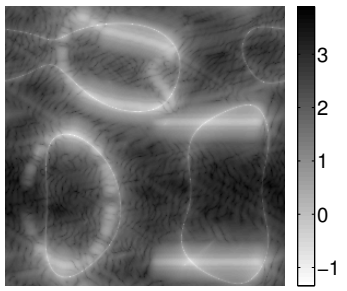	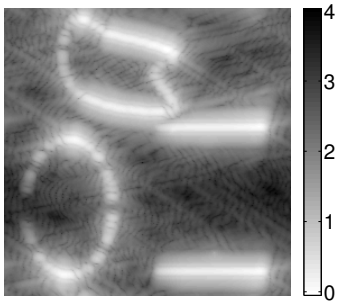
$\min_{\theta\in[0,2\pi)} d_{\theta,b}$	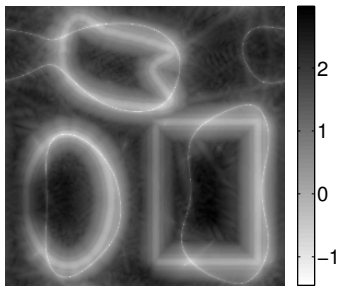	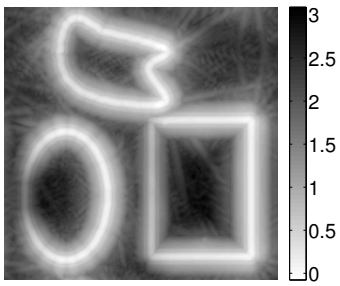

Figure 7. *Estimation of the regularity by decay rates of curvelet coefficients. The upper image shows the test image. The first two rows display the decay rates over two different orientations, that is, the functions* $I(b_1, b_2) = d_{\theta,(b_1,b_2)}$ *for* $\theta = \pi/8$ *and* $\theta = 5\pi/8$. *The bottom row shows the minimum of the decay rates, that is, the function* $I(b_1, b_2) = \inf_{\theta\in[0,2\pi)} d_{\theta,(b_1,b_2)}$. *As isotropic scales* $a_j \geq \alpha_0$ *are also considered for the estimation, the unstable amplitude of the CCT at the isotropic scales results in artifacts (thin curved lines), whereas the MCT does not suffer from this problem. Note that these artifacts do not occur if we take only the anisotropic scales* $a_j < \alpha_0$ *for the estimation of* $d_{\theta,(b_1,b_2)}$.

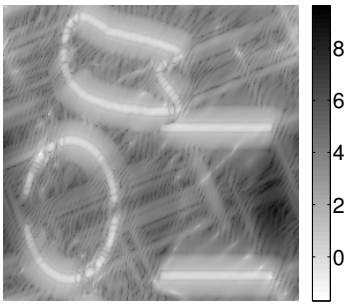

(a) Estimation of $d_{\pi/8,b}$ by the usual curvelet transform using all three anisotropic scales.

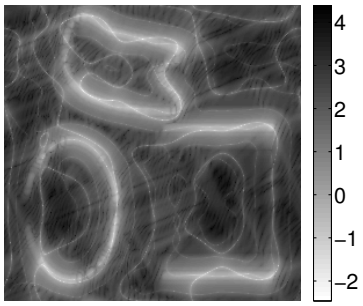

(b) Estimation of $d_{\pi/8,b}$ by the usual curvelet transform using all three anisotropic scales and the two subsequent isotropic scales.

(c) Estimation of $d_{\pi/8,b}$ by the MCT using all three anisotropic scales and the two subsequent isotropic scales.

Figure 8. *Estimation of $d_{\pi/8,b}$ by the curvelet transform with four directions at the finest scales. The estimation by the usual curvelet transform* (a) *using only the anisotropic scales oscillates strongly. Using also the subsequent two isotropic scales* (b) *results in artifacts as explained in Figure 7. The estimation by the MCT using the anisotropic and two subsequent isotropic scales is much smoother than the result of* (a) *and does not suffer from the artifacts of* (b).

is defined by $\overline{h} = \overline{a + \mathbf{i}\,b + \mathbf{j}\,c + \mathbf{k}\,d} = a - \mathbf{i}\,b - \mathbf{j}\,c - \mathbf{k}\,d$, and the absolute value is $|h| = \sqrt{h\overline{h}} = |a + \mathbf{i}\,b + \mathbf{j}\,c + \mathbf{k}\,d| = \sqrt{a^2 + b^2 + c^2 + d^2}$. The real part is denoted by $\operatorname{Re} h = a$ and the imaginary part by $\operatorname{Im} h = \mathbf{i}\,b + \mathbf{j}\,c + \mathbf{k}\,d$.[1]

Appendix B. Proof of Theorem 4.1.

We need the following lemma.

Lemma B.1. *Let $f, g \in L^2\left(\mathbb{R}^2, \mathbb{R}\right)$ such that $g \star g \star f \in L^2\left(\mathbb{R}^2, \mathbb{R}\right)$. Then*

$$\mathcal{F}(\mathcal{M}g \star \mathcal{M}g \star f) = 2\widehat{g}(\xi)^2 \widehat{\mathcal{M}f}(\xi).$$

Proof. Recall that $\mathbf{i}\,\mathbf{j} = -\mathbf{j}\,\mathbf{i}$. The claim follows from

$$\begin{aligned}
\mathcal{F}\left(\mathcal{M}g \star \mathcal{M}g \star f\right)(\xi) &= \mathcal{F}\left(g - \mathbf{i}\,\mathcal{R}_1 g - \mathbf{j}\,\mathcal{R}_2 g\right)(\xi) \mathcal{F}\left(g - \mathbf{i}\,\mathcal{R}_1 g - \mathbf{j}\,\mathcal{R}_2 g\right)(\xi) \widehat{f}(\xi) \\
&= \left(\widehat{g}(\xi) - \mathbf{i}\,\widehat{\mathcal{R}_1 g}(\xi) - \mathbf{j}\,\widehat{\mathcal{R}_2 g}(\xi)\right) \left(\widehat{g}(\xi) - \mathbf{i}\,\widehat{\mathcal{R}_1 g}(\xi) - \mathbf{j}\,\widehat{\mathcal{R}_2 g}(\xi)\right) \\
&= \widehat{g}(\xi)^2 \widehat{f}(\xi) \left(1 - \mathbf{i}\,i\,\frac{\xi_1}{|\xi|} - \mathbf{j}\,i\,\frac{\xi_2}{|\xi|}\right) \left(1 - \mathbf{i}\,i\,\frac{\xi_1}{|\xi|} - \mathbf{j}\,i\,\frac{\xi_2}{|\xi|}\right) \\
&= \widehat{g}(\xi)^2 \widehat{f}(\xi) \Bigg(1 - \mathbf{i}\,i\,\frac{\xi_1}{|\xi|} - \mathbf{j}\,i\,\frac{\xi_2}{|\xi|} - \mathbf{i}\,i\,\frac{\xi_1}{|\xi|} + \frac{\xi_1^2}{|\xi|^2} + \mathbf{i}\,\mathbf{j}\,i^2\,\frac{\xi_1\xi_2}{|\xi|^2} - \mathbf{j}\,i\,\frac{\xi_2}{|\xi|} \\
&\qquad + \mathbf{j}\,\mathbf{i}\,i^2\,\frac{\xi_1\xi_2}{|\xi|^2} + \frac{\xi_2^2}{|\xi|^2}\Bigg) \\
&= \widehat{g}(\xi)^2 \widehat{f}(\xi) \left(2 - 2\mathbf{i}\,i\,\frac{\xi_1}{|\xi|} - 2\mathbf{j}\,i\,\frac{\xi_2}{|\xi|}\right) \\
&= 2\widehat{g}(\xi)^2 \left(\widehat{f}(\xi) + \mathbf{i}\,\widehat{\mathcal{R}_1 f}(\xi) + \mathbf{j}\,\widehat{\mathcal{R}_2 f}(\xi)\right) \\
&= 2\widehat{g}(\xi)^2 \widehat{\mathcal{M}f}(\xi). \qquad \blacksquare
\end{aligned}$$

[1] Note the difference from a complex number z: $\operatorname{Im} z$ is real, whereas $\operatorname{Im} h$ is imaginary.

Proof of Theorem 4.1. We mainly follow the argumentation of [5]. Let

$$g_{a\theta}(x) := \int_{\mathbb{R}^2} \langle \mathcal{M}\beta_{ab\theta}, f\rangle \, \mathcal{M}\beta_{ab\theta}(x)\, db$$

in $L^2(\mathbb{R}^2, \mathbb{R})$. We have to show

$$\mathcal{M}f(x) = \int_0^\infty \int_0^{2\pi} g_{a\theta}(x)\, d\theta\, da/a^3 \tag{B.1}$$

in $L^2(\mathbb{R}^2, \mathbb{R})$. Let $\widetilde{\ }$ denote the reflection. As $\mathcal{M}\beta_{ab\theta}(x) = \mathcal{M}\beta_{a0\theta}(x-b)$, we have

$$\begin{aligned} g_{a\theta}(x) &= \int_{\mathbb{R}^2} \mathcal{M}\beta_{a0\theta}(x-b) \left(\int_{\mathbb{R}^2} \overline{\mathcal{M}\beta_{a0\theta}(y-b)} f(y)\, dy \right) db \\ &= \int_{\mathbb{R}^2} \mathcal{M}\beta_{a0\theta}(x-b) \left(\overline{\widetilde{\mathcal{M}\beta}_{a0\theta}} \star f \right)(b)\, db \\ &= \mathcal{M}\beta_{a0\theta} \star \overline{\widetilde{\mathcal{M}\beta}_{a0\theta}} \star f(x) \\ &= \mathcal{M}\beta_{a0\theta} \star \mathcal{M}\beta_{a0\theta} \star f(x), \end{aligned}$$

because $\widehat{\beta}_{a0\theta}$ is symmetric with respect to the origin and real-valued and hence $\widetilde{\mathcal{M}\beta}_{a0\theta}(x) = \mathcal{M}\beta_{a0\theta}(-x) = \overline{\mathcal{M}\beta_{a0\theta}(x)}$. The preceding lemma yields

$$\widehat{g}_{a\theta}(x) = \mathcal{F}(\mathcal{M}\beta_{a0\theta} \star \mathcal{M}\beta_{a0\theta} \star f)(\xi) = 2\widehat{\beta}_{a0\theta}(\xi)^2 \widehat{\mathcal{M}f}(\xi).$$

Plugging this into (B.1), we get

$$\begin{aligned} \widehat{\mathcal{M}f}(\xi) &= \int_0^\infty \int_0^{2\pi} \widehat{g}_{a\theta}(\xi)\, d\theta\, da/a^3 \\ &= 2\widehat{\mathcal{M}f}(\xi) \int_0^\infty \int_0^{2\pi} \widehat{\beta}_{a0\theta}(\xi)^2\, d\theta\, da/a^3. \end{aligned}$$

So it remains to show that

$$\int_0^\infty \int_0^{2\pi} \widehat{\beta}_{a0\theta}(\xi)^2\, d\theta\, da/a^3 = 1/2. \tag{B.2}$$

We split the integral into two parts:

$$\int_0^\infty \int_0^{2\pi} \widehat{\beta}_{a0\theta}(\xi)^2\, d\theta\, da/a^3 = \int_0^{a_0} \int_0^{2\pi} \widehat{\beta}_{a0\theta}(\xi)^2\, d\theta\, da/a^3 + \int_{a_0}^\infty \int_0^{2\pi} \widehat{\beta}_{a0\theta}(\xi)^2\, d\theta\, da/a^3.$$

As $\widehat{\beta}_{a0\theta}$ is defined in polar coordinates, we rewrite the equation via $\xi = r(\cos\omega, \sin\omega)$ to get

$$\widehat{\beta}_{a0\theta}(\xi) = \frac{1}{2} W(ar) V\left(\frac{\omega - \theta}{\sqrt{a}} \right) a^{3/4};$$

thus

$$\int_0^{a_0}\int_0^{2\pi} \widehat{\beta}_{a0\theta}(\xi)^2\, d\theta\, da/a^3 = \int_0^{a_0}\int_0^{2\pi} \frac{1}{2} W(ar)^2 a^{3/2} V\left(\frac{\omega-\theta}{\sqrt{a}}\right)^2 d\theta\, da/a^3. \tag{B.3}$$

The admissibility condition for V yields

$$\int_0^{2\pi} V\left(\frac{\omega-\theta}{\sqrt{a}}\right)^2 d\theta = a^{1/2}.$$

So (B.3) reduces to

$$\frac{1}{2}\int_0^{a_0} W(ar)^2\, da/a.$$

For the second part we have

$$\begin{aligned}\int_{a_0}^{\infty}\int_0^{2\pi} \widehat{\beta}_{a0\theta}(\xi)^2\, d\theta\, da/a^3 &= \int_{a_0}^{\infty}\int_0^{2\pi} \frac{1}{4} W(ar)^2 \frac{a^2}{\pi}\, d\theta\, da/a^3 \\ &= \int_{a_0}^{\infty} \frac{1}{2} W(ar)^2\, da/a \quad \forall r = |\xi| \text{ with } \xi \in \operatorname{supp} \widehat{f}.\end{aligned}$$

After summing up the two integrals, we get from the admissibility condition

$$\frac{1}{2}\int_0^{\infty} W(ar)^2\, da/a = \frac{1}{2}\int_0^{\infty} W(t)^2 \frac{r}{t}\, dt/r = \frac{1}{2}\int_0^{\infty} W(t)^2\, dt/t = \frac{1}{2},$$

which completes the proof of (4.2). Now we prove the Parseval formula. Writing the inner product as a convolution and applying the Plancherel formula, we get

$$\begin{aligned}\int |\langle \mathcal{M}\beta_{ab\theta}, f\rangle|^2\, db\, d\theta\, da/a^3 &= \int \left|(\overline{\mathcal{M}\beta_{a0\theta}} \star f)(b)\right|^2 db\, d\theta\, da/a^3 \\ &= \int \left\|(\overline{\mathcal{M}\beta_{a0\theta}} \star f)\right\|_2^2 db\, d\theta\, da/a^3 \\ &= \int \left\|\widehat{(\overline{\mathcal{M}\beta_{a0\theta}}\widehat{f})}\right\|_2^2 d\theta\, da/a^3 \\ &= \int \left|\widehat{\beta}_{a0\theta}(\xi)\left(1 + \mathbf{i}\, i\, \frac{\xi_1}{|\xi|} + \mathbf{j}\, i\, \frac{\xi_2}{|\xi|}\right)\right|^2 \left|\widehat{f}(\xi)\right|^2 d\xi\, d\theta\, da/a^3 \\ &\quad \int \left|\widehat{\beta}_{a0\theta}(\xi)\right|^2 \left(\sqrt{1 + \frac{\xi_1^2}{|\xi|^2} + \frac{\xi_2^2}{|\xi|^2}}\right)^2 \left|\widehat{f}(\xi)\right|^2 d\xi\, d\theta\, da/a^3 \\ &= \int 2\left|\widehat{\beta}_{a0\theta}(\xi)\right|^2 \left|\widehat{f}(\xi)\right|^2 d\xi\, d\theta\, da/a^3 \\ &= 2\int \left|\widehat{f}(\xi)\right|^2 \left(\int \left|\widehat{\beta}_{a0\theta}(\xi)\right|^2 d\theta\, da/a^3\right) d\xi \\ &= 2\int \left|\widehat{f}(\xi)\right|^2 \frac{1}{2}\, d\xi = \|f\|_2^2,\end{aligned}$$

where the last line follows from (B.2). ∎

REFERENCES

[1] P. Abry, P. Gonçalvès, and J. L. Véhel, eds., *Scaling, Fractals and Wavelets*, ISTE, London, Wiley, Hoboken, NJ, 2009.

[2] T. Bülow and G. Sommer, *Hypercomplex signals—a novel extension of the analytic signal to the multidimensional case*, IEEE Trans. Signal Process., 49 (2001), pp. 2844–2852.

[3] E. Candès, L. Demanet, D. Donoho, and L. Ying, *Fast discrete curvelet transforms*, Multiscale Model. Simul., 5 (2006), pp. 861–899.

[4] E. J. Candès and D. L. Donoho, *Continuous curvelet transform.* I. *Resolution of the wavefront set*, Appl. Comput. Harmon. Anal., 19 (2005), pp. 162–197.

[5] E. J. Candès and D. L. Donoho, *Continuous curvelet transform.* II. *Discretization and frames*, Appl. Comput. Harmon. Anal., 19 (2005), pp. 198–222.

[6] E. J. Candès and D. L. Donoho, *New tight frames of curvelets and optimal representations of objects with piecewise C2 singularities*, Comm. Pure Appl. Math., 57 (2004), pp. 219–266.

[7] M. Felsberg and G. Sommer, *The monogenic signal*, IEEE Trans. Signal Process., 49 (2001), pp. 3136–3144.

[8] S. L. Hahn, *Hilbert Transforms in Signal Processing*, Artech House, Boston, 1996.

[9] S. Held, M. Storath, P. Massopust, and B. Forster, *Steerable wavelet frames based on the Riesz transform*, IEEE Trans. Image Process., 19 (2010), pp. 653–667.

[10] L. Jacques and J.-P. Antoine, *Multiselective pyramidal decomposition of images: Wavelets with adaptive angular selectivity*, Int. J. Wavelets Multiresolut. Inf. Process., 5 (2007), pp. 785–814.

[11] F. W. King, *Hilbert Transforms*, Vol. 1, Encyclopedia Math. Appl. 124, Cambridge University Press, Cambridge, UK, 2009.

[12] F. W. King, *Hilbert Transforms*, Vol. 2, Encyclopedia Math. Appl. 125, Cambridge University Press, Cambridge, UK, 2009.

[13] N. Kingsbury, *Image processing with complex wavelets*, Philos. Trans. R. Soc. Lond. Ser. A Math. Phys. Eng. Sci., 357 (1999), pp. 2543–2560.

[14] J. Ma and G. Plonka, *The curvelet transform: A review of recent applications*, IEEE Signal Process. Magazine, 27 (2010), pp. 118–133.

[15] S. Mallat, *A Wavelet Tour of Signal Processing. The Sparse Way*, Elsevier/Academic Press, Amsterdam, 2009.

[16] S. C. Olhede and G. Metikas, *The monogenic wavelet transform*, IEEE Trans. Signal Process., 57 (2009), pp. 3426–3441.

[17] J. Sampo and S. Sumetkijakan, *Estimation of Hölder regularities and direction of singularity by Hart Smith and curvelet transforms*, J. Fourier Anal. Appl., 15 (2009), pp. 58–79.

[18] I. W. Selesnick, R. G. Baraniuk, and N. C. Kingsbury, *The dual-tree complex wavelet transform*, IEEE Signal Process. Magazine, 22 (2005), pp. 123–151.

[19] E. M. Stein, *Singular Integrals and Differentiability Properties of Functions*, Princeton University Press, Princeton, NJ, 1970.

[20] M. Storath, *The monogenic curvelet transform*, in Proceedings of the IEEE International Conference on Image Processing (ICIP), Hong Kong, 2010.

[21] M. Unser, D. Sage, and D. Van De Ville, *Multiresolution monogenic signal analysis using the Riesz-Laplace wavelet transform*, IEEE Trans. Image. Process., 18 (2009), pp. 2402–2418.

[22] M. Unser and D. Van De Ville, *Higher-order Riesz transforms and steerable wavelet frames*, in Proceedings of the IEEE International Conference on Image Processing (ICIP), Cairo, 2009, pp. 3801–3804.

[23] S. Yi, D. Labate, G. R. Easley, and H. Krim, *A shearlet approach to edge analysis and detection*, IEEE Trans. Image Process., 18 (2009), pp. 929–941.

[24] L. Ying, L. Demanet, and E. Candes, *3D discrete curvelet transform*, in Proceedings of the SPIE, Vol. 5914 (Wavelets XI), San Diego, 2005.